Transition State Structure in Cycloaddition Reactions as a Function of Ring Size and Geometry

Henry S. Rzepa* and William A. Wylie
Department of Chemistry, Imperial College of Science, Technology and Medicine, London, SW7 2AY, UK
E-mail: RZEPA@UK.AC.IC.CH.VAXA

The relative energies of the stepwise one-bond and synchronous two-bond reaction pathways are compared at the semi-empirical AM1 and PM3 SCF and *ab initio* MP2 levels for the closed shell $_{\pi}2_s + _{\pi}4_s$ cycloaddition reaction between the NO_2^+ ion and ethyne. The intrinsic bias towards the stepwise route for this reaction is estimated at 11 kcal mol^{-1} for PM3 and rather more for AM1.† There is reasonable agreement between the AM1 and PM3 geometries and those obtained using *ab initio* MCSCF methods for the $_{\pi}2_s + _{\pi}4_s$ reaction between ethene and butadiene, the $_{\pi}2_s + _{\pi}2_a$ cyclodimerisation of ethene, and the $_{\pi}2_s + _{\pi}2_s$ reaction between ethene and ketene. The location of two second-order saddle points for the latter reaction, where the antarafacial component is located on either the ethene or the ketene, allows the antarafacial stabilisation *via* the carbonyl group to be estimated as 27 kcal mol^{-1}. The effect of *E*/*Z* isomerism and of antarafacial components on the geometries and energies of the synchronous stationary points for a range of larger ring cycloadditions is established at the AM1 and PM3 levels. The prediction by McIver that such reactions will become increasingly asynchronous as the ring size increases is only weakly manifested at the closed shell RHF SCF level, but is more prominent at the spin unrestricted UHF level. The crossover between synchronous and asynchronous bond formation probably occurs for ten-membered rings.

The suggestion by McIver[1] that the transition states for cycloaddition reactions should tend towards asymmetry with increasing ring size has provoked much attention over the years. The original argument was based on a consideration of the relative magnitude of the interaction force constant (f_{12}) and the stretching force constants (f_{11} or f_{22}) for the two bonds r_1 and r_2 involved in the reaction (Scheme 1). For cases where $r_1 = ca.\ r_2$, the relationship $f_{11} > f_{12}$ should be increasingly true as the ring size increases. If so, the corresponding (2 by 2) force constant matrix would necessarily have two negative and, in the limit, degenerate roots, and the stationary point for the geometry $r_1 = ca.\ r_2$ would be a second-order saddle point (SOSP) and not a true transition state.

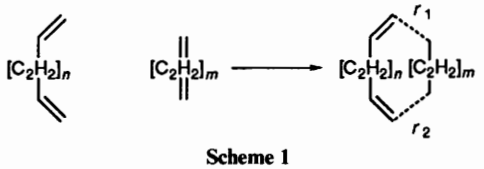

Scheme 1

The first quantitative normal coordinate analyses were performed at the MINDO/2[2] and MINDO/3[3] closed shell SCF–MO levels for the transition state **1** corresponding to the $_{\pi}2_s + _{\pi}4_s$ reaction between butadiene and ethene. The calculated Hessian matrices, expressed in cartesian coordinates, in each case had two negative roots corresponding to symmetric (ν_1) and antisymmetric (ν_2) combinations of the r_1 and r_2 stretches. This result implied that the McIver effect could be manifested even for six-membered rings, but numerous subsequent calculations at both single (SCF) and subsequently multi-configurational (MCSCF) *ab initio* levels[4] for five- and six-membered $_{\pi}2_s + _{\pi}4_s$ additions show that the Hessian matrix for the symmetrical structure has only one negative root corresponding to the mode ν_1. These early semi-empirical results are now thought to be the result, at least in part, of overestimating the core–core or the electron–electron repulsions in the C–C region 2.0–2.5 Å.[5] Others have argued that the inherent features of the NDDO approximations intrinsically favour unsymmetrical transition states.[6] More recent semi-empirical parametrisations such as AM1[5] or PM3[7] have addressed the core–core repulsion problem, and these methods do allow a genuinely symmetrical transition state ($r_1 = ca.\ r_2$) at the RHF–SCF level, at least for six-membered rings. Less attention has been given to antarafacial pathways, but recent *ab initio* MCSCF calculations for *e.g.* the synchronous route for $_{\pi}2_a + _{\pi}2_s$ dimerisation of ethene or its reaction with ketene[8] indicate that for such topology the force constant for the ν_2 mode is negative, and the reaction proceeds instead along asynchronous biradicaloid pathways. We present here semi-empirical AM1 and PM3 calculations for a range of cycloadditions which assess the impact of ring size, and of the presence of *E*/*Z* isomerism and antarafacial components on the synchronous stationary point geometries.

Computational Procedure.—Initial estimates of the stationary point geometries were obtained by molecular mechanics minimisation using either the Macromodel (V3.0) program[9] or the Tektronix CAChe workstation system and employing the MM2(85) hydrocarbon force field. The variables r_1 and r_2 were constrained to 2.12 Å by assigning to them large stretching force constants. All other force field parameters were unchanged from the MM2 values. For large ring systems where the number of *E*/*Z* permutations is large, less favourable isomers were eliminated on the basis of the molecular mechanics calculations. The approximate geometries obtained were then expressed in terms of an appropriate set of $3N - 6$ internal coordinates, and re-optimised at the AM1 or PM3 level whilst maintaining the constraint on r_1 and r_2, using the MOPAC (V5.0 and more recently V6.0) program[10] implemented on Vaxstation 3200, RS 6000/530 or CAChe workstations. Finally all the $3N - 6$ internal coordinates were re-optimised by minimising the sum of their squared scalar gradients (keyword NLLSQ), followed by calculation of the force constant matrix

† 1 cal = 4.184 J.

Table 1 Calculated AM1 and PM3 properties of cycloaddition reactions as a function of ring size

Entry[a]	Mode	AM1 $E(v_1, v_2)$[b]	AM1 r_1, r_2[c]	PM3 $E(v_1, v_2)$[b]	PM3 r_1, r_2[c]
RHF					
1	$_{\pi}2_s + {}_{\pi}4_s$	23.0 (−9.51, 147)	2.12, 21.2	26.3 (−937, 151)	2.14, 2.14
5	$_{\pi}2_s + {}_{\pi}2_a$	70.8 (−1167, −214)	2.10, 2.10	74.0 (−1325, −275)	2.13, 2.10
11 *Z, Z*	$_{\pi}4_s + {}_{\pi}4_a$	52.7 (−1763, −130)	2.07, 2.10	54.3 (−1761, −77)	2.07, 2.11
12 *E, Z*	$_{\pi}4_s + {}_{\pi}4_a$	54.2 (−1655, −183)	2.07, 2.09	57.5 (−1668, −36)	2.07, 2.09
13 *Z, Z*	$_{\pi}4_s + {}_{\pi}6_s$	40.8 (−1818, 5)	2.09, 2.21	42.5 (−1775, 49)	2.06, 2.19
14 *E, Z*	$_{\pi}4_s + {}_{\pi}6_s$	38.2 (−1981, −121)	2.08, 2.13	39.7 (−1916, 64)	2.10, 2.11
UHF					
15	$_{\pi}2_s + {}_{\pi}4_s$	21.1 (−804, −223)	2.11, 2.12	24.5 (−762, −112)	2.14, 2.16
16 *Z, Z*	$_{\pi}4_s + {}_{\pi}4_a$	39.2 (−854, −651)	2.06, 2.11	40.1 (−850, −679)	2.10, 2.11
17 *E, Z*	$_{\pi}4_s + {}_{\pi}4_a$	41.6 (−847, −700)	2.06, 2.06	44.0 (−818, −682)	2.08, 2.08
18 *Z, Z*	$_{\pi}4_s + {}_{\pi}4_s$	24.1 (−783, −657)	2.07, 2.08	27.1 (−752, −567)	2.13, 2.14
19 *E, E*	$_{\pi}4_s + {}_{\pi}4_s$	27.9 (−771, −672)	2.08, 2.08	31.1 (−734, −624)	2.11, 2.11
20 *Z, Z/Z*	$_{\pi}4_s + {}_{\pi}6_s$	22.5 (−709, −588)	2.10, 2.12	26.8 (−653, −525)	2.15, 2.17
21 *Z, E/Z*	$_{\pi}4_s + {}_{\pi}6_s$	20.4 (−707, −602)	2.10, 2.11	24.5 (−673, −553)	2.14, 2.15
22 *Z/Z, Z/Z*	$_{\pi}6_s + {}_{\pi}6_s$	18.0 (−722, −673)	2.09, 2.09	22.5 (−667, −611)	2.13, 2.13
23 *Z/Z, Z/Z*	$_{\pi}6_s + {}_{\pi}6_a$	26.9 (−690, −644)	2.10, 2.11	31.3 (−644, −593)	2.14, 2.15
24 *E/Z, E/Z*	$_{\pi}6_s + {}_{\pi}6_s$	21.1 (−724, −605)	2.09, 2.09	24.1 (−664, −605)	2.13, 2.14
25 *Z/Z, E/Z*	$_{\pi}6_s + {}_{\pi}6_a$	27.7 (−659, −565)	2.10, 2.15	32.5 (−632, −536)	2.13, 2.19
26 *E/Z, E/Z/E*	$_{\pi}6_a + {}_{\pi}8_a$	18.5 (−673, −638)	2.10, 2.11	20.0 (−637, −594)	2.15, 2.15
27 *E/Z, Z/E/E*	$_{\pi}6_s + {}_{\pi}8_s$	16.4 (−690, −659)	2.08, 2.09	18.8 (−622, −582)	2.14, 2.14

[a] The nomenclature for the *E/Z* isomers is based on the final product geometry. [b] Calculated enthalpy of activation in kcal mol^{-1} and vibrational wavenumbers in cm^{-1} in parentheses. Imaginary modes are shown as negative numbers. All barriers are relative to the corresponding ground state. [c] Bond lengths in Å.

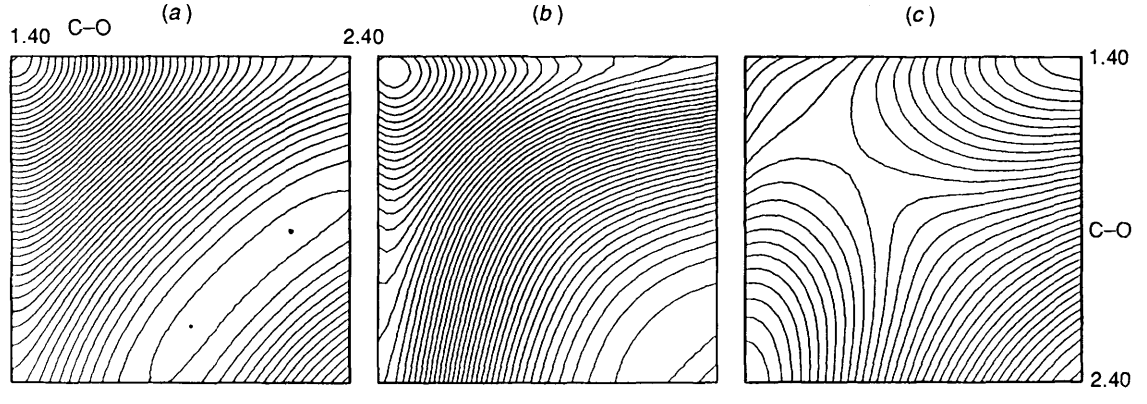

Fig. 1 Potential energy surfaces for the $_{\pi}2_s + {}_{\pi}4_s$ reaction between HCCH and O_2N^+ as a function of r_1 and r_2 at (*a*) PM3, (*b*) AM1 levels and (*c*) as a difference map. Contour levels are separated by 0.5 kcal mol^{-1}.

and normal coordinate analysis. Final values of the gradient norms were <1 kcal Å^{-1}. Where location of true transition states was desired, the eigenvector following method recently implemented in MOPAC[11] was employed. *Ab initio* calculations were performed using the GAUSSIAN 86 program system,[12] transition states being located using the eigenvector following implementation due to Baker.[13] Molecular coordinates in the form of Gaussian archive files and MOPAC cartesian coordinates have been deposited for located stationary points [Sup. pub. no. 56832 (14 pp.)]. Normal mode diagrams were generated using the Molecule program.[14]

Results and Discussion

(i) $_{\pi}2_s + {}_{\pi}4_s$ *Cycloaddition.*—The calculated AM1 and PM3 properties (Table 1) for the transition state **1** are similar to those reported at the *ab initio* level.[4] Likewise, the calculated normal mode v_2 corresponding to the antisymmetric distortion ($r_1 - r_2$) is real at both AM1[5] (147 cm^{-1}) and the PM3 (151 cm^{-1}) RHF levels. No numerical value for this mode at the multi-configurational (MCSCF) *ab initio* level has been reported.[4] The semi-empirical value may be distorted by several effects; intrinsic bias towards asymmetrical structures as a result of the NDDO approximations,[6] variation in the AM1 or PM3 parameters themselves[15] or the use of a closed shell wavefunction in which any biradicaloid character introduced from asymmetrical distortion of **1** is not included.[5] We followed two strategies to try to assess these two effects separately. The first was to investigate charged systems for which the one-bond stepwise reaction ($r_1 \neq r_2$) and the two-bond synchronous reaction ($r_1 = r_2$) are formally both closed shell species and can therefore at least qualitatively be compared using the same SCF level formalism. The closest analogy to transition state **1** would be from the reaction between allyl cation and ethene, but this system proved unsuitable because of the very early nature of the transition state and the corresponding low barrier (*ca.* 1 kcal mol^{-1}). Instead we chose as our model the $_{\pi}2_s + {}_{\pi}4_s$ reaction between ethyne and the electrophilic nitronium ion NO_2^+ (Scheme 2). This system has the advantage of a low number of degrees of

Table 2 Calculated properties for the cycloaddition of ethyne to O_2N^+ or O_2B^-

	O_2N^+		O_2B^-	
	Energy[a]	ν_1, ν_2[b]	Energy[a]	ν_1, ν_2[b]
AM1	288.4 (14.6)	−411, −86	−34.5 (81.2)	−970, −353
PM3	291.3 (34.0)	−527, 42	—	—
6-31 + G	−280.3113 (11.6)	−462, 134	−251.1140 (105.5)	−1023, −115
6-31*	−280.4683 (25.5)	−617, 199	−251.1624 (116.0)	−1124, −337
6-31 + G*	−280.4736 (27.6)	−632, 194	−251.2016 (112.4)	−1138, −327
MP2/6-31G	−280.9591 (12.2)	−628, 321	−251.6132 (88.4)	−919, −74
MP2/6-31 + G	−280.9724 (13.7)	—	−251.6711 (81.8)	−852, 89
MP2/6-31G*	−281.3328 (4.5)	−631, 307	−251.9291 (78.4)	−1020, −356

[a] In kcal mol^{-1} for AM1 and PM3, in Hartree for the *ab initio* calculations. The energy of the stationary point relative to the ground state reactants is given in parentheses in kcal mol^{-1}. [b] Vibrational wavenumbers, in cm^{-1} for the first two normal modes.

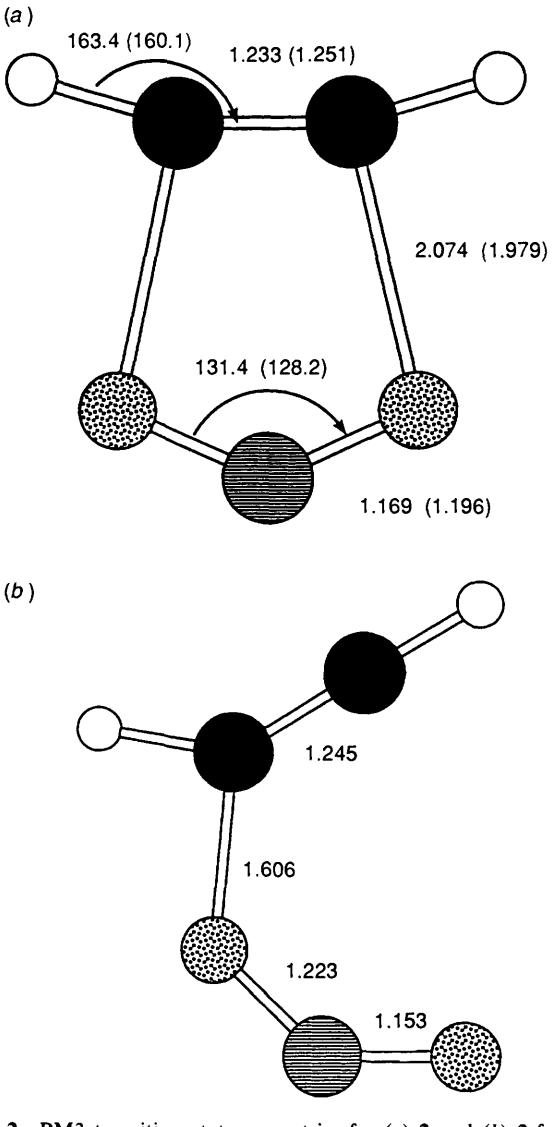

Fig. 2 PM3 transition state geometries for (*a*) **2** and (*b*) **3** for the reaction between O_2N^+ and HCCH. Bond lengths in Å with MP2/6-31G* values in parentheses.

freedom, which allows *ab initio* calculations up the MP2/6-31G* level to be carried out within reasonable computing resources (Table 2).

A PM3 contour map of energy against r_1 and r_2 reveals the presence of a genuine synchronous transition state (**2**, Fig. 1*a*), although a stepwise route is also available leading to a transition state **3** which is 3.0 kcal mol^{-1} lower in energy than **2**. This contrasts with the AM1 surface, which reveals **2** to be a second-order saddle point [Fig. 1(*b*)] having two negative force constants. The difference in the two surfaces (Fig. 1*c*) is clearly attributable to the parameters, as both parametrisations are based on the same approximations. In particular, we have previously noted a specific error in the AM1 nitrogen parametrisation which is not found in PM3.[15] Qualitatively similar geometries to those obtained using PM3 were found at the *ab initio* SCF and MP2 levels (Fig. 2) and ν_2 for **2** was similarly real. Although a significant *ab initio* basis set effect on the relative energy of **2** is evident, the frequencies of ν_1 and ν_2 were less affected (Table 2). Most significantly, ν_2(MP2/6-31G*) is *ca.* 270 cm^{-1} greater than the corresponding PM3 value for this mode. The *ab initio* calculations do differ qualitatively from PM3 in that no MP2/6-31G saddle point corresponding to **3** could be located, despite extensive searching using eigenvector following techniques.[13] From the calculated MP2/6-31G energy of this system at O–C bond lengths of 2.0–1.9 Å, the energy in the stepwise region of the potential surface is estimated as being 8 kcal mol^{-1} *higher* than in the synchronous region. We conclude that, for the formation of C–O bonds at least, PM3 has a bias of *ca.* 11 kcal mol^{-1} against the *energy* of the symmetrical structure, manifested in a value of ν_2 that is *ca.* 270 cm^{-1} lower than the *ab initio* value (Table 2). The AM1 method shows greater divergence, **3** being 7.7 kcal mol^{-1} lower than **2**, with an error in ν_2 of 393 cm^{-1}. Nevertheless, the energy bias against symmetrical structures has been a feature of all semi-empirical parametrisations, and it seems unlikely that this is due to the parameters alone. This is also supported by our results for the simplest of all two-bond reactions, a proton transfer between two heteroatoms. We have previously observed[16] that the PM3 or AM1 errors in the calculated transfer barriers were of the order of 20 kcal mol^{-1}. These are of a magnitude that seems unlikely to be due to the values of the parameters alone and may instead be due to the inherent NDDO approximations[6] or the limited orbital basis set employed in these methods.

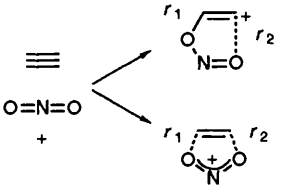

Scheme 2

It is possible to perturb the system such that **3** becomes lower in energy than **2** and in the process a genuine transition state. The BO_2^- anion is isoelectronic to the NO_2^+ cation, and identical with respect to the forming C–O bonds, but the calculated reaction barrier is much higher since the reactants are both nucleophilic (Table 2). In this case modes ν_1 and ν_2 for the symmetrical geometry are both imaginary at all levels of theory. For this specific case, good agreement is obtained

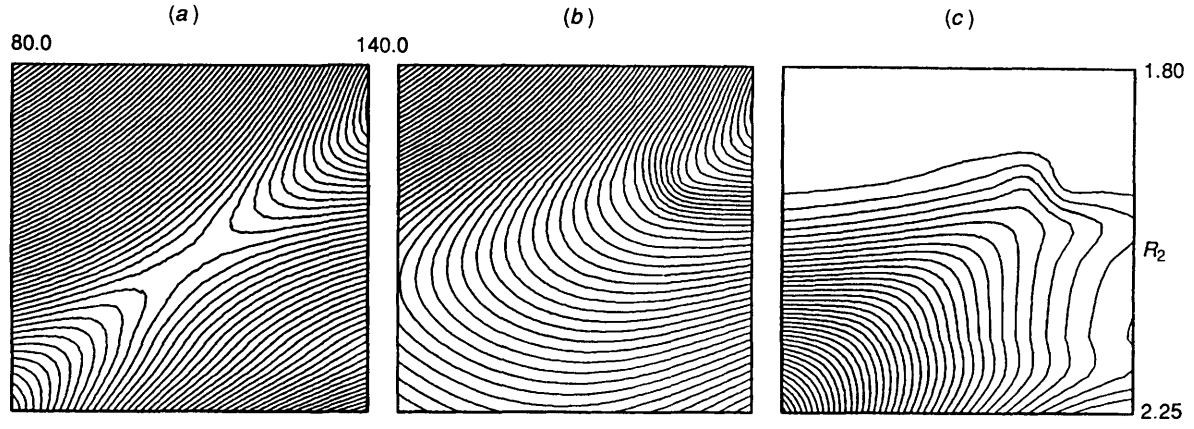

Fig. 3 PM3 energy contour maps for the ${}_{\pi}2_s + {}_{\pi}2_a$ dimerisation of ethene as a function of the distance r_m between the two C–C bond mid-points and the dihedral angle γ between the two planes defined by the three atoms of the terminal methylene groups, at (*a*) the RHF, (*b*) the UHF level and (*c*) as a difference map between (*a*) and (*b*). C_2 symmetry was maintained throughout and contour levels are separated by 1 kcal mol^{-1}.

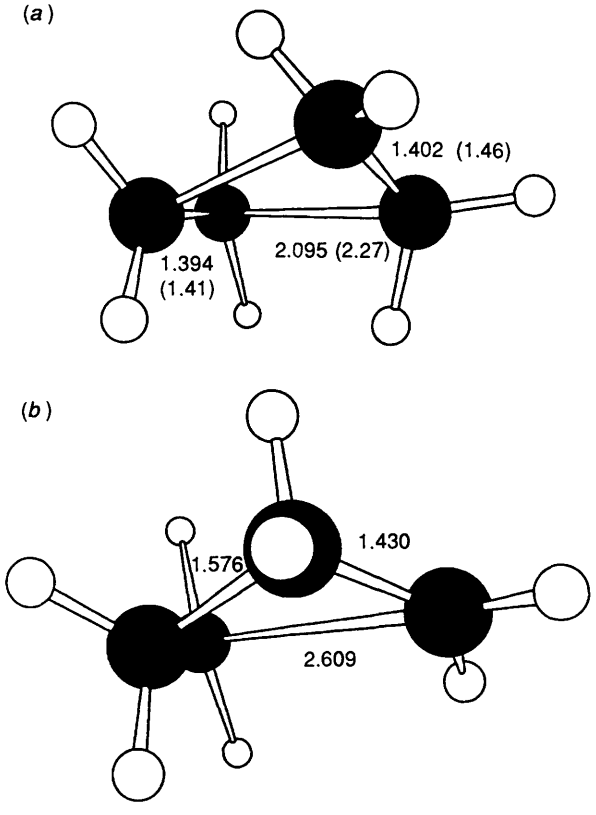

Fig. 4 Calculated PM3 geometry of (*a*) the second-order saddle point point **5** (bond lengths in Å, with the corresponding MCSCF/4-31G values in parentheses) and (*b*) **6**

between the AM1 and the highest level *ab initio* calculations, although the barrier to reaction is so high that a bias of *ca.* 10 kcal mol^{-1} in the semi-empirical result might not be apparent.

All alternative perturbation may derive from geometrical constraints in the transition state itself. In other work,[17] we have noted that the ${}_{\pi}2_s + {}_{\pi}4_s$ transition state **4** has significant ring strain induced by the particular stereochemistry of this system. This strain is manifested in a substantially unsymmetrical PM3 geometry (r_{C-C} 1.61, r_{C-N} 2.67 Å), whereas

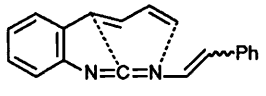

4

unstrained stereoisomers have similar values for r_1 and r_2. A similar induction of asymmetry was observed in certain six-electron dihydrogen transfer reactions from di-imide to highly strained bridgehead alkenes.[18]

Our second strategy was to consider the effect that the use of a closed shell wavefunction in which biradicaloid character is excluded might have on the symmetry of transition state **1**. The simplest formalism which allows approximate biradical character in a wavefunction is the unrestricted Hartree–Fock (UHF) approach.[19] At this level, the re-optimised stationary point **15** is no longer a true transition state, both ν_1 and ν_2 being imaginary at the AM1 and the PM3 levels (Table 1).[19b] Compared with the PM3–RHF results, the UHF energy lowering (1.8 kcal mol^{-1}), change in geometry and degree of biradical character for **1** ($\langle s^2 \rangle$ = *ca.* 0.5) are small, but the change in ν_2 (−263 cm^{-1}) is more significant (Table 1). More rigorous treatments at the *ab initio* MCSCF level[4] indicate the symmetrical structure **1** still to be a genuine transition state, but with little biradicaloid character. The absence of a reported value for ν_2 at the MCSCF level as noted above does not permit comment regarding the effect of the UHF approximation on this normal mode. However, such results are available for the related ${}_{\pi}2_s + {}_{\pi}2_a$ dimerisation of ethene or its reaction with ketene, which we consider next.

(ii) ${}_{\pi}2_s + {}_{\pi}2_a$ *Cycloaddition.*—At the MCSCF/4-31G level,[8] the symmetrical stationary point for the dimerisation of ethene (**5**) has been reported as having imaginary values for both normal modes ν_1 and ν_2 (1072i and 327i cm^{-1} respectively) with $r_1 = r_2 = 2.27$ Å. The formal antarafacial component is accommodated *via* a dihedral angle φ of 40.8° between the two reactant C–C bonds and by the relative twisting (γ *ca.* 90°) of the two methylene groups of *one* reactant ethene. AM1 or PM3 energy contour maps of γ against the mid-point separation, r_m, of the two reactant C–C bonds show an apparent saddle point in this region (Fig. 3*a*), with a geometry which reveals (Fig. 4) an antarafacial distortion similar to the *ab initio* MCSCF values [φ 36.0° (PM3), 42.5° (AM1)]. The effect of the RHF approximation is seen in the calculated length of the C–C antarafacial bond, which is noticeably shorter than the MCSCF value (Fig. 4). As found previously,[8] **5** is not a true transition state since the ν_2 mode is imaginary, and the contour map shows a saddle point only because C_2 symmetry was imposed. The AM1 or PM3 force constant corresponding to ν_2 is less negative than the MCSCF value (Table 1), possibly because of the use of a single determinantal wavefunction. Despite the significant twisting in one alkene component there is nevertheless good agreement between the semi-empirical

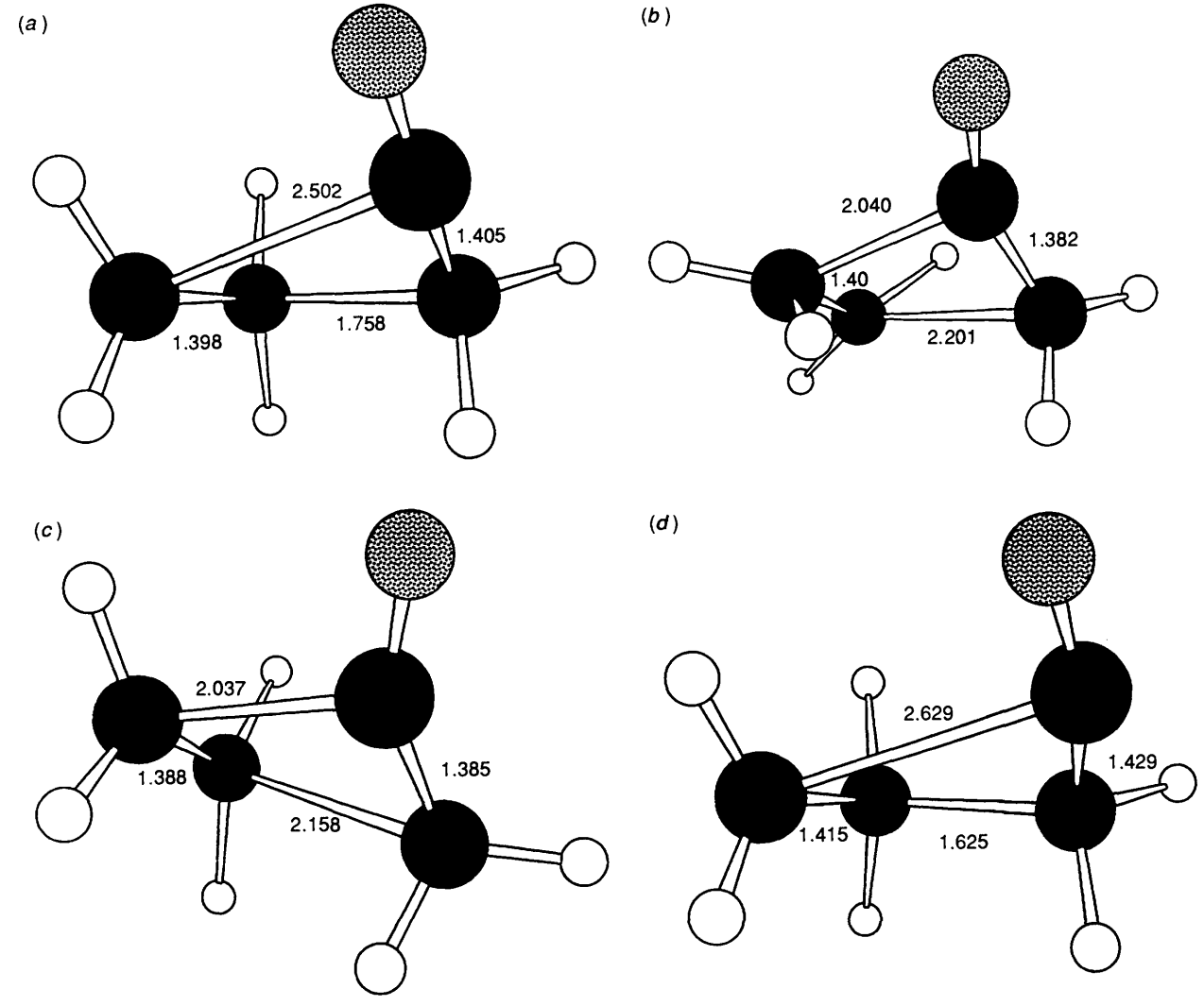

Fig. 5 Calculated PM3 geometries for stationary points (*a*) **7**, (*b*) **8**, (*c*) **9** and (*d*) **10**

Table 3 PM3 HOMO and LUMO energies (eV) for Structures **1**, **5** and **11–14**

Entry	E_{HOMO}	E_{LUMO}
1	−9.02	0.34
5	−8.75	0.204
11	−7.91	0.17
12	−8.14	−0.43
13	−7.76	−0.84
14	−7.95	−0.71

closed shell and the *ab initio* MCSCF results for **5**. Inspection of the HOMO–LUMO gap (Table 3) reveals it to be only slightly less than that for **1** itself, and therefore that qualitatively similar geometries at the SCF and MCSCF level for this reaction are not entirely unexpected.[20] The calculated barrier to **5** is substantial (Table 1), but when the v_2 mode is followed using eigenvector following techniques,[11] a genuine transition state **6** (r_1 = 1.576/1.584, r_2 = 2.609/2.609 Å, PM3/AM1) can be located (Fig. 4*b*) with an accompanying energy lowering of 11.5/11.7 kcal mol^{-1}. Structure **6** clearly has major biradical characteristics[4] and when such character is introduced into the semi-empirical wavefunction using the UHF approximation, the potential surface for the dimerisation of ethene does change (Fig. 3*b*), most significantly in regions where r_m is >2 Å and the relative twisting of one alkene component is close to 90° (Fig. 3*c*). This introduces a new stationary point corresponding to $_\pi2_s + _\pi2_s$ addition (r_m *ca.* 2.1 Å, γ *ca.* 0°) and the resultant distortion of the potential surface in this region removes the $_\pi2_s + _\pi2_a$ second-order saddle point previously observed. Since this stationary point persists at the more rigorous *ab initio* MCSCF level, this semi-empirical result must be considered an artifact of the UHF approximation.

Further comparison with *ab initio* MCSCF calculations is possible for the ketene + ethene cycloaddition, which has been extensively studied theoretically.[8] We were able to locate *two* second-order saddle points at the PM3/RHF level, the first (**7**, Fig. 5*a*) being analogous to the *ab initio* structure, with the antarafacial component clearly located on the ketene, and the second previously uncharacterised[8] point (**8**, Fig. 5*b*) having the antarafacial component located on the ethene. Comparison of the calculated semi-empirical and *ab initio* MCSCF properties (Table 4) shows qualitative agreement between the two approaches in predicting the C–C bond in **7** to be shorter than the C–CO bond length. By following the PM3 v_2 mode for **7** in one direction we were able to locate a genuine transition state (**9**, Fig. 5*c*) which was 3.5 kcal mol^{-1} lower in energy. The values for the C–C and C–CO bond lengths for this transition state are approximately equal (Fig. 5) at the PM3 level but less equal at the AM1 level (Table 4). However, given the propensity of semi-empirical methods to disfavour a symmetrical structure in favour of an unsymmetrical alternative (*cf.* **2** *vs.* **3** above), and the observation that SCF and MCSCF methods show *least* divergence for symmetrical structures (*cf.* **5**), it may

Table 4 AM1 and PM3 properties for the $_{\pi}2_s + _{\pi}2_a$ cycloaddition between ethene and ketene

	AM1		PM3	
Entry	$E(v_1, v_2)$[a]	r_{C-C}, r_{C-CO}[b]	$E(v_1, v_2)$[a]	r_{C-C}, r_{C-CO}[b]
7	45.2 (−957, −121)	1.729, 2.483	46.3 (−982, −269)	1.757, 2.502
7			(−1447, −403)[c]	2.08, 2.36[d]
9	39.7 (−780, 164)	2.454, 1.731	42.8 (−1150, 149)	2.158, 2.037
			−226.7122[e]	1.888, 2.325
			−229.6820[f]	1.756, 2.441
			−227.0438[g]	1.960, 2.320
10	45.2 (−877, 121)	1.700, 2.515	45.8 (−578)	1.625, 2.629
8	72.0 (−1236, −274)	2.220, 2.004	73.1 (−1308, −286)	2.201, 2.040

[a] Calculated enthalpy of activation in kcal mol^{-1} and vibrational wavenumbers in cm^{-1} in parentheses. Imaginary modes are shown as negative numbers. [b] Bond lengths in Å. [c] MCSCF/STO-3G values.[8] [d] MCSCF/4-31G values.[8] [e] SCF/3G calculation. [f] SCF/6-31G* calculation. [g] MP2/3G calculation.

indeed be possible that **9** has an analogue at the MCSCF level in addition to the unsymmetrical gauche transition states already located.[8] We also note that where asynchronous bond formation is predicted at the *ab initio* SCF level, allowance for dynamic electron correlation (*e.g.* the MP2 correction) tends to result in more synchronous structures, as for example the Beckmann rearrangement.[15] To check this, we carried out *ab initio* calculations for **9** at the minimal STO-3G and 6-31G* basis level (Table 4). Application of the MP2 correction at the STO-3G level does indeed symmetrise the transition state somewhat, but use of a larger basis at the SCF level decreases the symmetry. A 6-31G*/MP2 level calculation was precluded by the computational resources available to us.

The possibility that the symmetry of **9** is an artifact of the PM3 potential surface should also be considered. In particular, the properties of **4** noted above seem to indicate that PM3 predicts either essentially synchronous or highly asynchronous bond formation, with no intermediate continuum of structures. This might well be a feature of the parametrisation scheme, in which between two and four attractive or repulsive gaussian functions are used to modify the basic core–core repulsion function.[5] An erroneous value for the mid-point of one of these functions is responsible for the AM1 nitrogen error previously discussed,[15] and such faults also cause ridges in the AM1 phosphorus potential.[20] A less discernible ridge in the PM3 C–C potential might distort a modestly unsymmetrical saddle point towards either more (*i.e.* **9**) or less (*i.e.* **4**) symmetrical species. To resolve these two explanations, MCSCF calculations at *e.g.* the MP2 level of theory[21] are probably needed to establish whether a genuine $_{\pi}2_s + _{\pi}2_a$ transition state for the ethene + ketene cycloaddition actually exists. Following the PM3 v_2 mode of **7** in the opposite direction results in a less contentious and highly unsymmetrical transition state **10** (Fig. 5*d*) more akin to the gauche transition states[8] referred to above.

The structure of the alternative saddle point **8** [Fig. 5(*b*)] is similar to that of the analogous **5** and is 26.8 kcal^{-1} higher in energy than **7**, which provides a measure of the stabilisation of the antarafacial component across the ketene *via* involvement of the previously orthogonal p_{π} orbitals from the carbonyl group. Following the v_2 mode in **8** results in a pair of true transition states [r_{C-C} 1.568, r_{C-CO} 2.735 or r_{C-C} 2.793, r_{C-CO} 1.537 Å (PM3); r_{C-C} 1.571, r_{C-CO} 2.627 or r_{C-C} 2.760, r_{C-CO} 1.541 Å (AM1)] which are respectively 18.8, 13.1, 17.9 and 13.5 kcal mol^{-1} lower in energy. All these points are nevertheless > 11 kcal mol^{-1} higher than **9** showing that the lack of symmetry does not remove the preference of the antarafacial component for the ketene.

Several important conclusions can be drawn from these various results. At the AMI or PM3 RHF level, stationary point cycloaddition geometries involving either *supra* or *antarafacial* components in four-, five- or six-membered rings are qualitatively similar to those obtained by *ab initio* MCSCF calculations. For cycloadditions involving *e.g.* charged reactants where the wavefunction in both the synchronous and asynchronous regions of the potential surface is dominated by a closed shell configuration, the semi-empirical RHF force constant corresponding to antisymmetric distortion v_2 appears to be underestimated, the error being larger for AM1 than PM3. This error is compensated by this force constant being overestimated (*i.e.* too positive) for *e.g.* uncharged antarafacial mode reactions where other electronic configurations contribute significantly to, but do not dominate, the wavefunction. Use of the semi-empirical UHF approximation gives values of v_2 which are clearly too large (negative), but it remains to be established if this is still true for reactions where the RHF approximation breaks down completely. To investigate this aspect, we next applied the AM1 and PM3 Hamiltonians to a variety of larger ring cycloadditions, particularly with regard to the calculated geometries, energies and normal modes of the *symmetrical* stationary points (r_1 = *ca.* r_2). For such systems, *ab initio* calculations become increasingly expensive, and the utility of 'pathfinding' semi-empirical methods needs to be established.

(iii) *Larger Ring Reactions at the RHF Level.*—The effect of *E*/*Z* isomerism in the product cycloalkenes and the possibility of antarafacial modes of addition in the larger ring reactions render these geometrically much more complex than the simple Diels–Alder case **1**. At the closed shell RHF level, symmetrical stationary points (r_1 = *ca.* r_2) corresponding to either *Z*/*Z* or *E*/*Z* products were located for the $_{\pi}4_a + _{\pi}4_s$ (**11** and **12** respectively) and the $_{\pi}4_s + _{\pi}6_s$ systems (**13** and **14** respectively, Table 1). All the C–C bond lengths other than r_1 and r_2 were in the range 1.37–1.41 Å. For the eight-membered ring, the stationary point corresponding to a product with one *trans* double bond was energetically higher than the *cis* isomer, whilst the reverse was true for the ten-membered ring case. The calculated RHF barriers are significantly higher than for **1** and as the ring size increases, the HOMO–LUMO gap decreases to *ca.* 7 eV for **13** or **14** (Table 3). This trend eventually resulted in anomalous behaviour during attempts to locate a stationary point for the $_{\pi}6_s + _{\pi}6_a$ or $_{\pi}6_s + _{\pi}8_s$ reactions. In the expected saddle point region (r_1 = *ca.* r_2 = *ca.* 2.15 Å), pronounced bond alternation was observed, with discontinuous transition between reactants and products; a phenomenon clearly due to the closed shell approximation. For this reason, we think it unlikely that any genuine stationary points exist at the RHF level for these larger rings.

The McIver force constant argument predicts that as the ring size increases, the two normal modes v_1 and v_2 would eventually both become imaginary and degenerate. For the eight-membered rings in which an antarafacial mode is present (**11** and **12**), v_2 is indeed imaginary, although the force constants

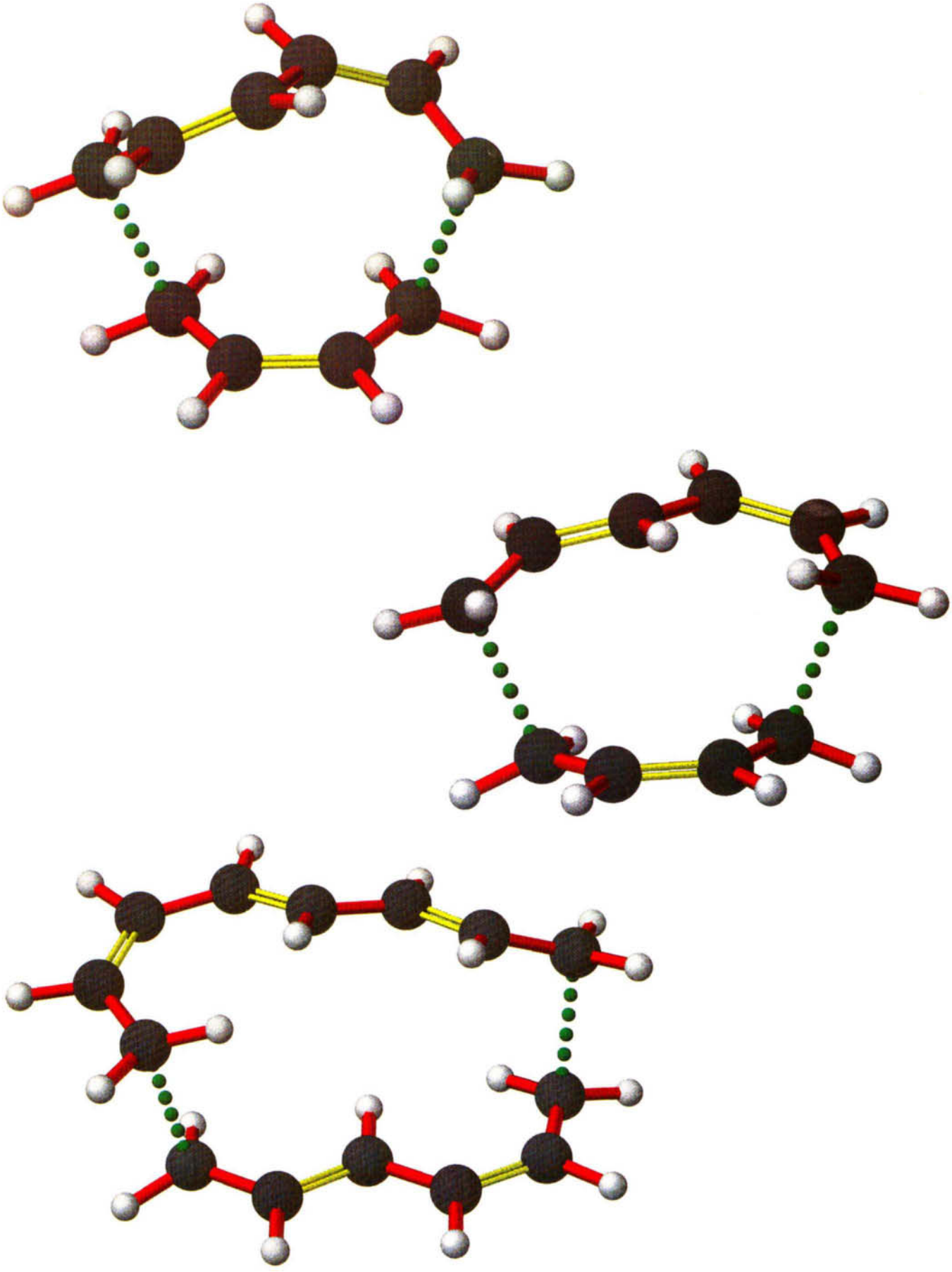

Fig. 6 Calculated PM3 UHF geometries for the suprafacial mode transition states **20**, **21** and **27**. Double bonds shown in yellow relate to those formed in the product, and do not indicate the bond orders in the transition state.

(Facing p. 944)

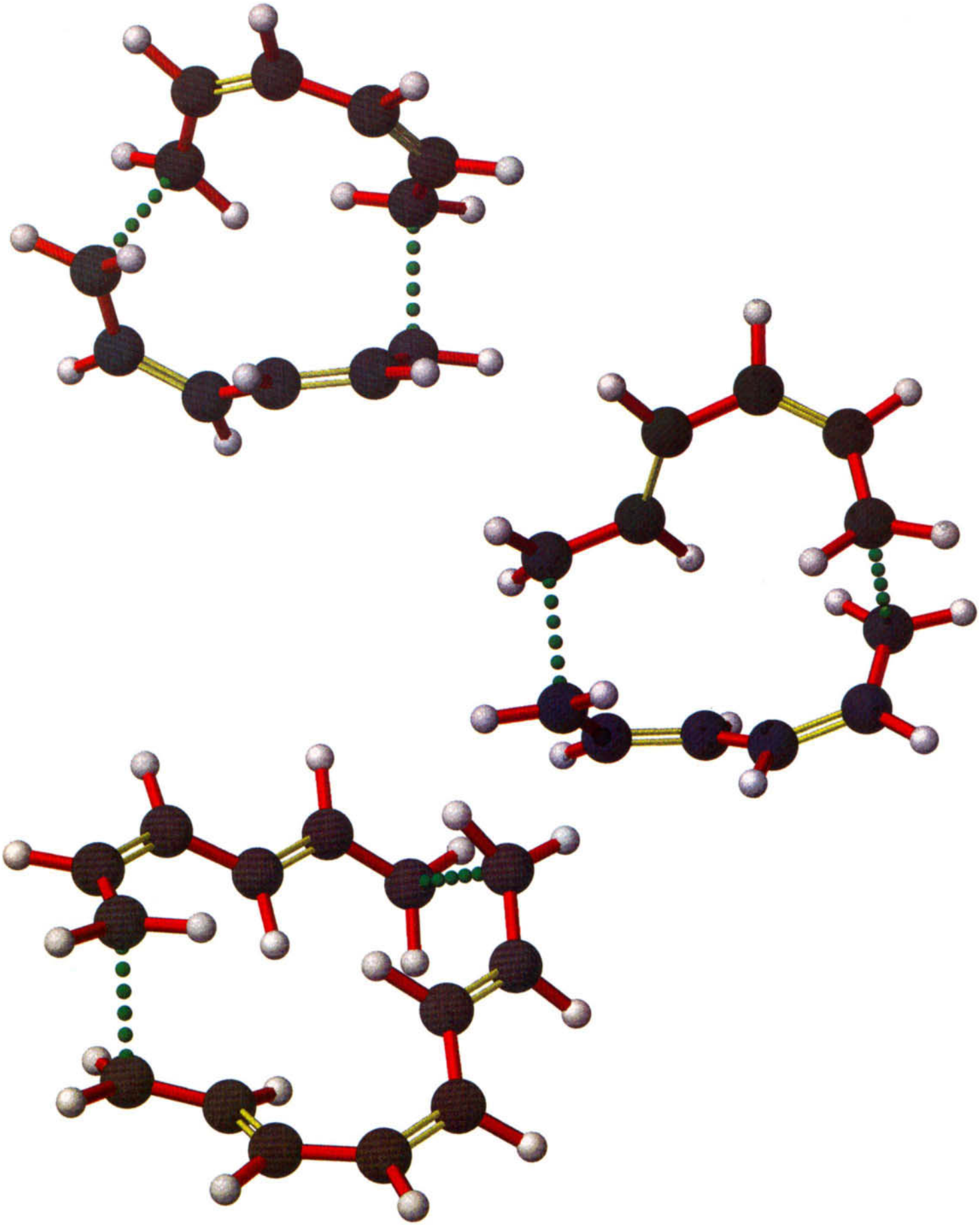

Fig. 7 Calculated PM3 UHF geometries for the antarafacial mode transition states **23**, **25** and **26**

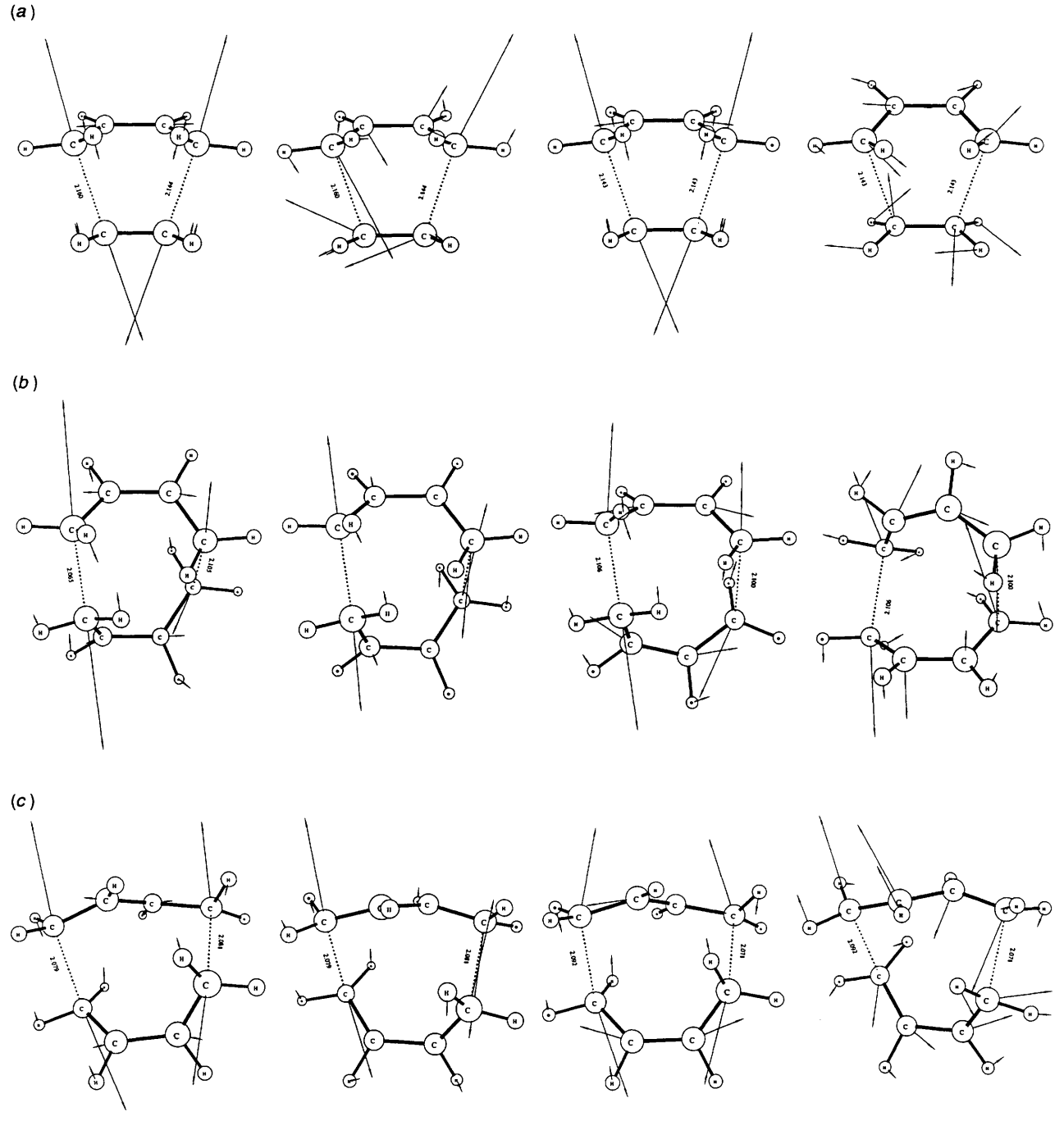

Fig. 8 Stationary point geometries and calculated form of the normal modes ν_1 and ν_2 for (*a*) **1** and **15**, (*b*) **11** and **16** and (*c*) **12** and **17**

are *less* negative than was found for the four-membered ring case, especially for PM3 (Table 1). However, ν_1 also increases substantially in both cases and there is no indication of ν_1 and ν_2 becoming degenerate. Thus at the AM1 level for **13** or **14**, the value of ν_2 decreases only modestly compared with its value in **1**, and with PM3 this 'McIver' effect is even less prominent, ν_2 being real rather than imaginary (Table 1). As noted above however, we expect the RHF approximation to result in too positive a value for the ν_2 force constant and this would become increasingly true as the difference in HOMO/LUMO energies becomes smaller. This decrease is particularly apparent for the ten-membered rings **13** and **14** (Table 3) and it seems probable that this ring size may represent the crossover point where cycloaddition reactions become inherently asynchronous.

(iv) *Larger Ring Reactions at the UHF Level.*—The decrease in the HOMO–LUMO energy gap for the larger rings suggests that the closed shell RHF approximation becomes increasingly inappropriate for these systems. Use instead of the UHF method in these instances results in continuous potential surfaces for all ring sizes, and enabled the 'allowed' ${}_{\pi}6_s + {}_{\pi}8_s$ (**27**) and ${}_{\pi}6_a + {}_{\pi}8_a$ (**26**) modes to be located as well as analogues to those previously located at the RHF level (**15**–**17**, **20**, **21**, Fig. 6). In common with the results described for **5**, the 'forbidden' ${}_{\pi}4_s + {}_{\pi}4_s$ (**18**, **19**) and ${}_{\pi}6_s + {}_{\pi}6_s$ (**22**, **24**) modes could also be located. Several of these stationary points involved antarafacial components (Table 1), suggesting that the failure noted above to locate the UHF equivalent of **5** (Fig. 3) was a particular result of the localisation of the antarafacial component across a single double bond. In the larger ring, the

antarafacial twisting is delocalised over four or more atoms, resulting in much less, if any strain (Fig. 7).

Direct comparison between the RHF and UHF stationary points is possible for the pairs **1**/**15**, **11**/**16**, **12**/**17**, **13**/**20**, **14**/**21** (Fig. 8). The calculated geometries and in particular the relative *E*/*Z* or supra/antarafacial energies are highly consistent. For example, the energy differences **12** − **11** (3.2) and **17** − **16** (3.9), or **14** − **13** (−2.8) and **21** − **20** (−2.3 kcal mol^{-1}) show that the UHF and RHF methods predict similar *E*/*Z* substituent effects, and the comparisons **11** − **13** (11.8) and **16** − **20** (13.3 kcal mol^{-1}) indicate that this is also true for the supra-antarafacial energy differences. More significantly, at the UHF level the values of the activation barriers are significantly lower, and the normal modes ν_1 and ν_2 are both imaginary for all ring sizes. Specifically, the ν_2 mode is often discernably different at the RHF and UHF level (Fig. 8). Within the UHF series **15**–**27**, the value of ν_1 gradually decreases whilst that of ν_2 rapidly approaches the value of ν_1. This is exactly the phenomenon predicted by McIver. However the UHF wavefunction contamination from triplet and higher spin states becomes more significant for the larger rings. This probably results in overestimation of the McIver effect, whereas the RHF calculations underestimate it. Another consequence of the UHF method is that the $_{\pi}4_s + {}_{\pi}4_s$ (**18**, **19**) and $_{\pi}6_s + {}_{\pi}6_s$ (**12**, **24**) 'forbidden' modes are now genuine stationary points, lower in energy than the 'allowed' antarafacial modes by 13.0 and 8.8 kcal mol^{-1} respectively. In reactions where there is no formal symmetry, the location of such 'forbidden' reactions is not precluded at the RHF level, as shown by the existence of both 'forbidden' and 'allowed' modes for the [1,2] methyl group migration in the Stevens rearrangement.[22] Nevertheless, it remains a possibility that **18**, **19**, **22** and **24** may be specific artifacts of the UHF method. Finally, we note that the *antara*/*antara* system **26** is not significantly disfavoured with respect to the *supra*/*supra* isomer **27**, indicating that in these large rings, such modes may be energetically quite accessible.

The structural similarities between the RHF and UHF structures for the 'allowed' stationary points, and the congruence with published *ab initio* MCSCF calculations noted above suggests that these semi-empirical calculations should provide valuable estimates of the geometries of such reactions. Whilst entropic considerations imply that in the absence of a catalyst the larger ring reactions are unlikely to be preferred to alternative smaller ring pathways, the use of *e.g.* abzymes for mediating such cycloadditions [23] provides an interesting indication of how such transformations might be accomplished, as well as suggesting a possible experimental probe for studying the symmetries of these reactions.

Acknowledgements

We thank D.E.N.I. for a studentship (to W. A. W.) and the SERC for the award of computing equipment grants for the Vaxstation and the CAChe workstation.

References

1 J. W. McIver, *Acc. Chem. Res.*, 1974, **7**, 73.
2 J. W. McIver and A. Komornicki, *J. Am. Chem. Soc.*, 1972, **94**, 2625.
3 M. J. S. Dewar, H. S. Rzepa and S. Olivella, *J. Am. Chem. Soc.*, 1978, **100**, 5650.
4 F. Bernardi, M. Olivucci and M. A. Robb, *Acc. Chem. Res.*, 1990, **23**, 405; F. Bernardi, A. Bottoni, M. J. Field, M. F. Guest, I. H. Hillier, M. A. Robb and A. Venturini, *J. Am. Chem. Soc.*, 1988, **110**, 3050; J. H. W. McDouall, M. A. Robb, V. Niazi, F. Bernardi and H. B. Schlegel, *J. Am. Chem. Soc.*, 1987, **109**, 4642.
5 M. J. S. Dewar, J. J. P. Stewart and S. Olivella, *J. Am. Chem. Soc.*, 1986, **108**, 5771.
6 W. T. Borden, R. J. Loncharich and K. N. Houk, *Ann. Rev. Phys. Chem.*, 1988, **39**, 213.
7 J. J. P. Stewart, *J. Comput. Chem.*, 1989, **10**, 209, 221; J. J. P. Stewart, *J. Comp. Aided Mol. Design*, 1990, **4**, 1.
8 F. Bernardi, A. Bottoni, M. Olivucci, M. A. Robb, H. B. Schlegel and G. Tonachini, *J. Am. Chem. Soc.*, 1988, **110**, 5993; F. Bernardi, A. Bottoni, M. A. Robb and A. Venturini, *J. Am. Chem. Soc.*, 1990, **112**, 2106.
9 F. Mohamadi, N. J. G. Richards, W. C. Guida, R. Liskamp, M. C. Lipton, M. Caufield, G. Chang, T. Hendrickson and W. C. Still, *J. Comput. Chem.*, 1990, **11**, 440.
10 J. J. P. Stewart, MOPAC, Quantum Chemistry Program Exchange, University of Indiana, Bloomington, USA, Program 455.
11 J. Baker, F. Jensen, H. S. Rzepa and A. Stebbings, *Quantum Chemistry Program Exchange Bulletin*, 1990, **10**, 76.
12 Gaussian program systems available from Gaussian Inc., 4415 Fifth Avenue, Pittsburgh, PA, USA.
13 J. Baker, *J. Comput. Chem.*, 1986, **7**, 385.
14 D. K. Agrafiotis, A. Streitwieser and H. S. Rzepa, *Quantum Chemistry Program Exchange Bulletin*, 1989, **9**, Program 583, with local modifications by M. Yi.
15 L. Grierson, M. J. Perkins and H. S. Rzepa, *J. Chem. Soc., Chem. Commun.*, 1987, 1779; H. S. Rzepa, *J. Chem. Res.*, 1988, 224; P. A. Hunt and H. S. Rzepa, *J. Chem. Soc., Chem. Commun.*, 1989, 623; I. Juranic, H. S. Rzepa and M. Yi, *J. Chem. Soc., Perkin Trans. 2*, 1990, 877; H. S. Rzepa and M. Yi, *J. Chem. Soc., Perkin Trans. 2*, 1990, 943.
16 H. S. Rzepa and M. Yi, *J. Chem. Soc., Perkin Trans. 2*, 1991, 531.
17 H. S. Rzepa, P. Molina, M. Alajarin and A. Vidal, paper in preparation.
18 D. K. Agrafiotis and H. S. Rzepa, *J. Chem. Soc., Perkin Trans. 2*, 1989, 367; 475.
19 (*a*) M. J. S. Dewar, S. Olivella and H. S. Rzepa, *Chem. Phys. Lett.*, 1977, **47**, 80; (*b*) J. Y. Choi and I. Lee, *J. Chem. Soc., Faraday Trans. 2*, 1989, **85**, 867.
20 H. S. Rzepa, *J. Chem. Soc., Perkin Trans. 2*, 1989, 2115; H. S. Rzepa and M. Yi, *J. Chem. Soc., Chem. Commun.*, 1989, 1502.
21 J. J. W. McDouall, K. Peasley and M. A. Robb, *Chem. Phys. Lett.*, 1988, **148**, 183.
22 D. K. Agrafiotis and H. S. Rzepa, unpublished results.
23 A. C. Braisted and P. G. Shultz, *J. Am. Chem. Soc.*, 1990, **112**, 7430.

Paper 1/00143D
Received 11*th January* 1991
Accepted 1*st March* 1991